

1

2

Structure of the human lipid-gated cation channel TRPC3

3

4

Chen Fan^{1*}, Wooyoung Choi^{1*}, Weinan Sun^{2,3}, Juan Du^{1#}, Wei Lü^{1#}

5

6

¹Van Andel Institute, 333 Bostwick Avenue N.E., Grand Rapids, Michigan 49503, USA.

7

²Vollum Institute, 3181 Sam Jackson Park Rd., Portland, OR 97239, USA

8

³Current address: Janelia Research Campus, 19700 Helix Drive, Ashburn, Virginia 20147, USA.

9

10

11

12

13 Running head. Architecture, domain arrangement, and ion-conducting pore of human TRPC3

14 **#CORRESPONDING AUTHOR**

15 Correspondence and requests for materials should be addressed to J. D. (email: juan.du@vai.org)

16 TEL: (616) 234-5358, FAX: 616-234-5170 or W. L. (email: wei.lu@vai.org). TEL: (616)

17 234-5022, FAX: 616-234-5170

18 *These authors contributed equally to this work.

19 **Abstract**

20 The TRPC channels are crucially involved in store-operated calcium entry and calcium
21 homeostasis, and they are implicated in human diseases such as neurodegenerative disease,
22 cardiac hypertrophy, and spinocerebellar ataxia. We present a structure of the full-length human
23 TRPC3, a lipid-gated TRPC member, in a lipid-occupied, closed state at 3.3 Angstrom. TRPC3
24 has four elbow-like membrane reentrant helices prior to the first transmembrane helix. The TRP
25 helix is perpendicular to, and thus disengaged from, the pore-lining S6, suggesting a different
26 gating mechanism from other TRP subfamily channels. The third transmembrane helix S3 is
27 remarkably long, shaping a unique transmembrane domain, and constituting an extracellular
28 domain that may serve as a sensor of external stimuli. We identified two lipid binding sites, one
29 being sandwiched between the pre-S1 elbow and the S4-S5 linker, and the other being close to
30 the ion-conducting pore, where the conserved LWF motif of the TRPC family is located.

31

32

33

34

35

36

37

38 **Introduction**

39 The cytosolic free Ca^{2+} concentration is strictly regulated because calcium is crucial to
40 most cellular processes, from transcription control, to neurotransmitter release, to hormone
41 molecule synthesis (Berridge et al., 2003; Kumar and Thompson, 2011; Sudhof, 2012). A major
42 mechanism regulating calcium homeostasis is store-operated calcium entry (SOCE), which is
43 triggered by the depletion of calcium stored in the endoplasmic reticulum (ER) (Ong et al., 2016;
44 Smyth et al., 2010). This process activates store-operated channels (SOCs) in the plasma
45 membrane, resulting in the influx of calcium that refills the calcium stores of the ER for further
46 cellular stimulation (Prakriya and Lewis, 2015). A key component of SOCE has been identified
47 as the TRPC channels, which are calcium-permeable, nonselective cation channels belonging to
48 the TRP superfamily (Liu et al., 2003; Zhu et al., 1998; Zhu et al., 1996).

49 Among the seven members in TRPC family, TRPC3, TRPC6, and TRPC7 are the closest
50 homologues, and they are unique in being activated by the lipid secondary messenger
51 diacylglycerol (DAG), a degradation product of the signaling lipid phosphatidylinositol
52 4,5-bisphosphate (PIP2) (Itsuki et al., 2012; Tang et al., 2001). However, the molecular
53 mechanism of such activation remains elusive due to a lack of knowledge of the lipid binding
54 sites. TRPC3, TRPC6, and TRPC7 share several functional domains, including N-terminal
55 ankyrin repeats (AR), a transmembrane domain (TMD) with six transmembrane helices (S1-S6),
56 and a C-terminal coiled-coil domain (CTD). They also exhibit an unusually long S3 helix, but
57 the function of the S3 helix is poorly understood (Vazquez et al., 2004).

58 TRPC3 is abundantly expressed in the cerebellum, cerebrum, and smooth muscles, and it
59 plays essential roles in the regulation of neurogenesis and extracellular/intracellular calcium
60 signaling (Gonzalez-Cobos and Trebak, 2010; Li et al., 1999). Dysfunction of TRPC3 has been
61 linked to neurodegenerative disease, cardiac hypertrophy, and ovarian adenocarcinoma (Becker
62 et al., 2011; Kitajima et al., 2016; Yang et al., 2009). Although TRPC3 has wide pharmaceutical
63 applications in treatment of these diseases, drug development specifically targeting TRPC3 has
64 been limited due to the lack of understanding of its molecular activation mechanisms (Oda et al.,
65 2017; Xia et al., 2015). Here we report the structure of full-length human TRPC3 (hTRPC3) in a
66 lipid-occupied, inactive state at an atomic resolution of 3.3 Å using single-particle cryo-electron
67 microscopy (cryo-EM). Our structure revealed the first atomic view of TRPC3 channel and its
68 two lipid binding sites, providing insight into the mechanisms of lipid activation and regulation
69 of Ca²⁺ homeostasis.

70 **Results**

71 **Overall architecture**

72 The full-length hTRPC3 could be purified to homogeneity, and electrophysiology experiment
73 showed that the baculovirus-expressed hTRPC3 is functional in HEK293 cells. The
74 three-dimensional reconstruction of hTRPC3 was of sufficient quality to allow *de novo* modeling
75 of almost the entire protein (Figure 1, Figure 1 – figure supplement 1-3), with the exception of
76 the first 21 N-terminal residues; the region connecting the TRP helix and the C-terminal domain
77 (residues 688-757); the loop connecting the linker domain LD6 and LD7 (residues 281-291); and

78 the last 30 C-terminal residues. We identified two lipid-like densities, one sandwiched between
79 the pre-S1 elbow and the S4-S5 linker, and the other wedged between the P loop and S6 of the
80 adjacent subunit. Notably, we modeled two lipid molecules at these two sites, nevertheless, we
81 were not able to determine the identity of the lipids at current resolution. Interestingly, the TRP
82 helix is perpendicular to the S6, and the density of the hinge region is poorly defined, even
83 though both the TRP helix and S6 exhibit excellent densities (Figure 1a, b).

84 The structure of TRPC3 has a solely alpha-helical composition (Figure 1a-d). While
85 TRPC3 shares a similar architecture of the TMD with other TRPCs, the third transmembrane
86 helix, S3, is nearly twice as long as the S3 in any other DAG-insensitive TRPC channels
87 including TRPC1, TRPC4 and TRPC5 (Figure 1 – figure supplement 4). It elongates into the
88 extracellular space and connects to the S4 through a remarkably long loop, where a glycosylation
89 site is observed (Figure 1c, d). The extended S3 gives rise to the shape of TMD distinctive to
90 voltage-gated potassium channels or other TRP channels (Guo et al., 2017; Long et al., 2007;
91 Paulsen et al., 2016; Shen et al., 2016; Winkler et al., 2017) (Figure 1e). Four elbow-like pre-S1
92 domains extrude from the TMD and are completely buried in detergent micelles, where the lipid
93 1 density is located (Figure 1, 2b). The C-terminal coiled-coil domain (CTD) is reminiscent of
94 the TRPM4 and TRPM8 structures, having a coiled-coil “pole” domain in the four-fold
95 symmetry axis, and the “rib” helix penetrating into a “tunnel” composed by adjacent intracellular
96 domains (Figure 1f). This structure thus stabilizes the tetrameric assembly through hydrophobic
97 and polar interactions (Figure 1b, 2b) (Winkler et al., 2017; Yin et al., 2018). The ankyrin repeat

98 domain (ARD), located on the bottom of the channel and comprising four pairs of ARs, is
99 significantly smaller than the ARD of TRPA1 and NOMPC (Jin et al., 2017; Paulsen et al., 2016)
100 (Figure 2b, c).

101 **Transmembrane domain and lipid-binding sites**

102 The TMD of TRPC3 shares topology similar to that of other TRP channels and voltage-gated
103 ion channels, consisting of the S1-S4 domain and the pore domain arranged in a
104 domain-swapped manner (Figure 1e, 3a). Nevertheless, the distinct activation mechanism of
105 TRC3, TRPC6, and TRPC7 by DAG implies unique features of their TMD. Indeed, comparison
106 of the relative arrangement of the S1-S4 domains with the pore domain shows remarkable
107 differences between TRPC3 and TRPA1 or TRPM4, yet overall agreement with TRPV1 (Figure
108 3 – figure supplement 1). Detailed inspection of the TMD in TRPC3 reveals two unique features:
109 a large elbow-like pre-S1 domain harboring a lipid-binding site (lipid 1), and an unusually long
110 S3 helix forming an extracellular domain (ECD), along with the S1-S2 linker and S3-S4 linker
111 (Figure 3a, b).

112 The pre-S1 elbow, embedded in the lipid bilayer, consists of two half transmembrane
113 helices (half TM1 and half TM2). The half TM1 connects to LD9, which is the last alpha helix in
114 the LD; the half TM2 connects to the pre-S1 helix, a short alpha helix prior to S1 running
115 horizontally along the intracellular face of the membrane (Figure 2a, 3c, 3d). This unique
116 configuration pulls the intracellular half of S1 away from the pore center, resulting in a
117 hydrophobic pocket behind the pre-S1 elbow and surrounded by half TM1 and S1 (Figure 3c).

118 Moreover, the outward movement of S1 opens a window between itself and S5 from the adjacent
119 subunit, exposing the intracellular half of S4 and the S4-S5 linker, which are key regions for TRP
120 channel gating, to the lipid environment (Figure 3d).

121 Indeed, we observed a lipid-shaped density (lipid 1) in this pocket (Figure 3c, d). The head
122 group of lipid 1 is well defined in the density map, forming several hydrogen bonds and polar
123 interactions with residues in the LD9, the pre-S1 elbow, half TM1, and the S4-S5 linker, while the
124 two hydrocarbon tails are in contact with S1, S4, the pre-S1 elbow, and half TM1 (Figure 3e, f). A
125 similar pre-S1 elbow structure with lipid-like density has been observed in the *Drosophila*
126 mechanosensitive channel NOMPC (Jin et al., 2017). We suggest that this lipid site may be
127 crucially linked to channel activation, given its interaction with S4 and the S4-S5 linker. A
128 mutation in this region (T561A on S4) results in gain of function, causing abnormal Purkinje cell
129 development and cerebellar ataxia in moonwalker mice (Becker, 2014) (Figure 1 – figure
130 supplement 4).

131 We also identified a second lipid-like density (lipid 2) in the lateral fenestration of the pore
132 domain, wedged between the P loop and S6 of adjacent subunit and forming both hydrophobic and
133 hydrophilic interactions (Figure 3g, h). Specifically, G640 on S6, interacting directly with the
134 hydrocarbon tail of lipid 2, has been reported as a key determinant of lipid recognition in TRPC3.
135 Mutations of G640 to alanine or larger residues distinctly changed the sensitivity of channel to
136 lipid activators (Lichtenegger et al., 2018). Moreover, lipid 2 is in close contact with the LFW
137 motif on the P loop, which is highly conserved throughout the TRPC family and is crucial to

138 channel function (Figure 1 – figure supplement 4). Replacing this motif by three alanine residues
139 in TRPC5 and TRPC6 resulted in a nonfunctional channel (Strubing et al., 2003). Therefore, the
140 lipid 2 binding site likely represents another important modulation site. In addition to interaction
141 with lipid 2, the LFW motif forms multiple hydrophobic interactions within the pore domain and
142 therefore plays an important role in maintaining the proper structure of the pore domain (Figure
143 3i).

144 A second unique feature of TRPC3 is the remarkably long S3, stretching out into the
145 extracellular side and supporting the formation of the ECD (Figure 3a). Within the ECD we
146 observed a cavity-like feature (Figure 3j), with S3 and the S3-S4 linker as a “back wall and roof”,
147 and the S1-S2 linker forming the entrance. This cavity is located right above the lipid bilayer,
148 and its interior is filled with both charged and hydrophobic residues (Figure 3j). Moreover, a
149 tyrosine residue (Y589) in the loop connecting the S5 and the P loop plugs into the cavity (Figure
150 3i). We speculate that the cavity may serve as a binding site for small molecules and that binding
151 of small molecules may directly affect channel function through Y589, implying a role for the
152 ECD as a sensor of external stimuli. This is in line with the finding that Pyr3, a TRPC3-specific
153 inhibitor, likely binds to the extracellular side of the protein (Kiyonaka et al., 2009). Furthermore,
154 a glycosylation site (N404) is observed in the S1-S2 loop, consistent with the prediction that
155 TRPC3 is monoglycosylated in the extracellular side (Figure 3i) (Vannier et al., 1998). The site is
156 very close to the P loop, suggesting that the glycosylation status may affect channel activity, and
157 this is consistent with the report that N-linked glycosylation is a key determinant of the basal

158 activity of TRPC3 (Dietrich et al., 2003). Further studies are necessary to clarify the
159 physiological role of the ECD.

160 **TRP domain**

161 The TRP domain—the namesake region in the TRP channel located at the border between
162 the transmembrane domain and the intracellular domain—is crucially involved in signal
163 transduction and channel gating (Garcia-Sanz et al., 2007; Taberner et al., 2013). Similar to that
164 of TRPM4, the TRP domain consists of a TRP helix that runs nearly parallel along the
165 intracellular face of the membrane and a TRP re-entrant helix embedded in the lipid bilayer
166 (Autzen et al., 2018; Guo et al., 2017; Winkler et al., 2017) (Figure 4a). The TRP helix penetrates
167 into the tunnel formed by the S4-S5 linker of the TMD on the top and the LD9 of the linker
168 domain in the intracellular space on the bottom (Figure 4a), showing an apparently disengaged
169 connection to the S6 helix through a loop of the hinge region instead of a continuous alpha
170 helical structure as in TRPM4 (Figure 4b, e). While the densities for both S6 and TRP helix were
171 well defined, their linker region was surprisingly poorly defined, indicating a high flexibility
172 between the TRP helix and S6 (Figure 4b, 1b). The TRP helix forms an approximate right angle
173 to the S6, in strong contrast to the TRPV1, TRPA1, and TRPM4 structures whose TRP helices
174 form obtuse angles with S6 (Figure 4b-e). Such a unique configuration of TRP helix and S6 in
175 TRPC3 has two consequences. First, the upward tilting of the TRP helix allows itself
176 approaching to the S4-S5 linker, suggesting their tighter coupling in comparison to the other TRP
177 subfamily channels (Figure 4 f-h). Second, the C-terminus of the TRP helix is in close contact

178 with the lipid 1 site. Given the crucial role of TRP helix and S4-S5 linker in channel gating and
179 their possible involvement in voltage dependence (Nilius et al., 2005b), the interplay among the
180 TRP helix, the S4-S5 linker and the lipid 1 site may provide a molecular basis for the
181 lipid-sensitive gating mechanism of TRPC3 relative to other TRP subfamily channels (Itsuki et
182 al., 2012).

183 Furthermore, the TRP helix forms a series of polar and hydrophobic interactions with the
184 S4-S5 linker and the LD9 helix (Figure 4a). Specifically, the highly conserved tryptophan W673
185 is extensively coupled with the S4-S5 linker through interactions with G552, P553, and P546.
186 Mutation of the corresponding W673 in TRPV3 results in Olmsted syndrome (Ni et al., 2016), and
187 replacement of the corresponding residue in NOMPC results in a channel that has increased
188 current amplitude but is nonresponsive to mechanical stimuli (Jin et al., 2017). Mutation of the
189 corresponding tryptophan in TRPV1 abolishes channel activation in response to depolarization
190 (Gregorio-Teruel et al., 2014). Replacement of the corresponding G552 in TRPC4 and TRPC5 by
191 serine results in a constantly open channel (Beck et al., 2013). Another highly conserved
192 tryptophan residue in the TRP helix, W681, tightly packs with W322 in the LD9 (Figure 4a and
193 Figure 1 – figure supplement 4). Interestingly, the highly conserved R677 in the TRP helix is
194 close to the head group of lipid 1, and its replacement by histidine increases channel activity and
195 results in neuronal cell death and cerebellar ataxia, perhaps by affecting the binding of lipid 1
196 (Figure 4a) (Fogel et al., 2016).

197 **Ion-conducting pore**

198 The ion-conducting pore of TRPC3 is lined with an extracellular selectivity filter and an
199 intracellular gate, with a wide central vestibule in the middle (Figure 5a). The pore adopts a
200 closed conformation with the narrowest radius - at I658 and L654 on S6 close to the intracellular
201 exit - of less than 1 Å, thus preventing ion passage (Lichtenegger et al., 2013) (Figure 5b).
202 Presumably, the channel is trapped in a lipid-bound inactive state or the bound lipids are not the
203 activator DAG. The selectivity filter is defined by the backbone carbonyl oxygens of I613, F614
204 and G615 located in the P loop. The narrowest point at G615 has a radius of 2.1 Å, allowing
205 partially dehydrated ions to pass through (Figure 5b, c). Moreover, five acidic residues in the P
206 loop and the extracellular end of S6 in TRPC3 impose a negative electrostatic surface potential,
207 which is important for cation selectivity (Figure 5a, d). On the intracellular site, the inner surface
208 along the CTD and ARD contains acidic residues, giving rise to a negative charge and thus
209 providing a possible pathway by which cations can access the cytoplasm (Figure 5a, e).

210 Similar to other Ca²⁺-permeable TRP channels, an acidic residue, E618, is located at the
211 entrance of the selectivity filter. An E618Q mutation impedes the calcium permeability of
212 TRPC3, but it preserves monovalent permeation (Poteser et al., 2011) (Figure 5b). The
213 neutralization of the corresponding acidic amino acid on TRPV1 remarkably decreases channel's
214 permeability to divalent ions (Garcia-Martinez et al., 2000). By contrast, replacement of a
215 glutamine residue at the corresponding position (Q977) by an acidic amino acid in TRPM4,
216 which is a Ca²⁺-impermeable TRP channel, produced moderate Ca²⁺ permeability (Nilius et al.,
217 2005a). Thus, having an acidic residue close to the selectivity filter may represent a general

218 principle of permeability for divalent cations in nonselective Ca^{2+} -permeable TRP channels.

219 **The intracellular domain**

220 TRPC3 exhibits a similar intracellular domain composition as TRPA1, including a C-terminal
221 CTD and a N-terminal ARD. We found several unanticipated features that advance our
222 understanding of the molecular basis of TRPC family (Figure 6a). First, the ARD in TRPC3,
223 consisting of 4 ARs, is significantly shorter than that in TRPA1 (16 repeats). Second, instead of a
224 straight coiled-coil domain as in TRPA1, TRPC3 adopts the characteristic umbrella-like CTD
225 “pole” and “rib” domain of the TRPM family (Figure 6b, c). Interestingly, the turn from the pole
226 to the rib helix is where the ankyrin repeats end. Third, between the rib domain and TRP helix,
227 there is a linker domain that has remarkable structural similarities to the MHR4 (TRPM
228 homology region) domain in TRPM4 (Autzen et al., 2018; Guo et al., 2017; Winkler et al., 2017),
229 as well as to the linker domain in NOMPC (Jin et al., 2017). The location of the linker domain
230 suggests a role for signal transduction from ARD and CTD further to TMD. Overall, the TRPC3
231 forms a unique intracellular domain that has structural features characteristic of the TRPM,
232 TRPA, and NOMPC families. Although the functional role of the intracellular domain is yet
233 unknown, it clearly contributes to the channel assembly through three major interfaces. The first
234 interface is contributed by the vertical CTD pole helices of the four subunits winding into a
235 tetrameric coiled-coil assembly (Figure 6b, c). This is a common feature employed to specify
236 subunit assembly and assembly specificity within the voltage-gated ion channel superfamily
237 (Figure 6b, c). The second interface is formed by the horizontal CTD rib helix penetrating through

238 the tunnel composed of ARD and LD from neighboring subunits, thus tethering them together
239 (Figure 6c, d). Notably, the rib helix is rich in positively charged residues, forming multiple
240 interactions with the charged residues in the LD. The third interface is located between LD and
241 LD/pre-S1 elbow of the adjacent subunit (Figure 6e). All these interactions knit the tetramer
242 together.

243 **Discussion**

244 The TRPC3 structure displays several unique features. Distinct to the TRPM, TRPV or TRPA
245 channels whose TRP helix and S6 form a continuous alpha helical structure, the TRP helix in
246 TRPC3 is disengaged from the S6, and is in close contact to both the S4-S5 linker and lipid 1 site,
247 which perhaps links to the lipid-induced activation. The remarkably long S3 endows TRPC3 a
248 unique shape of TMD and frames the ECD in which a cavity may act as a binding site for small
249 molecules, suggesting a role for the ECD in sensing extracellular stimuli. We identified two lipid
250 binding sites, one buried in a pocket surrounded by the pre-S1 elbow, S1, and the S4-S5 linker,
251 and the other inserted into the lateral fenestration of the pore domain. Our structure provides a
252 framework for understanding the complex gating mechanism of TRPC3.

253 **Figure legends**

254 **Figure 1. Architecture of human TRPC3.** (a) Three-dimensional reconstruction viewed parallel
255 to the membrane. The transparent envelope denotes the unsharpened reconstruction. (b) Slice
256 view of the reconstruction showing the interior of the channel. (c-f) Atomic model of TRPC3

257 viewed parallel to the membrane (c-d), from the extracellular side (e), and from the intracellular
258 side (f). Each subunit is colored differently.

259 **Figure 2. Structure of a single subunit.** (a) The schematic representation of TRPC3 domain
260 organization. Dashed lines indicate the regions that have not been modeled. (b-c) Cartoon
261 representation of one subunit color-coded to match panel a.

262 **Figure 3. Transmembrane domain, extracellular domain, and lipid-binding sites.** (a) Domain
263 organization. The channel is shown in surface representation, with one subunit shown in cartoon
264 representation. The colors match those in Figure 2a. (b) Details of the transmembrane domain and
265 extracellular domain. (c-d) Pre-S1 elbow and binding site of lipid 1. The lipid molecule is buried
266 inside the pocket formed by pre-S1 elbow, S1, and the S4-S5 linker. Two adjacent subunits (blue
267 and yellow) are shown in both cartoon and surface representations. The lipid molecule is shown
268 as sticks. (e-f) Residues that interact with lipid 1 are shown in sticks, and protein is shown in
269 cartoon representation. Lipid density is shown in mesh. (g-h) Lipid 2 binds between S6 and the P
270 loop of adjacent subunits, which are in light blue and wheat. (i) Structure of the ECD. Key
271 residues forming the cavity is shown in sticks. Adjacent subunits are in light blue and wheat. (j)
272 Surface representation of the ECD, colored according to the electrostatic surface potential. The
273 color gradient is from -5 to 5 kT/e (red to blue).

274 **Figure 4. The TRP domain.** (a). Cartoon representation of the TRP helix, pre-S1 elbow, TMD,
275 and linker domain, showing their interaction. Lipid 1 is shown in sticks. W673 on the TRP helix

276 stacks with P553 and G552 forming a hydrogen bond with the backbone oxygen (dashed line) of
277 P546 on the S4-S5 linker. The side chain of R677 is in close contact with the head group of lipid
278 1. (b-e). The pore lining helix S6 and the TRP helix in TRPC3 (b), TRPV1 (c), TRPA1 (d), and
279 TRPM4 (e). The angle between the S6 and TRP helices are indicated; only two subunits are
280 shown for clarity. The hinge connecting the S6 and TRP helix is highlighted in red. (f-h)
281 Comparison of TRPC3 with TRPV1, TRPA1, and TRPM4, respectively, focusing on the S4, S5
282 and TRP helix. Structures are superimposed using backbone atoms in S4 and S5. TRPC3 is in
283 blue, whereas TRPV1, TRPA1 and TRPM4 are in red. Proteins are shown in ribbon
284 representation, and lipid 1 in TRPC3 is shown in sticks. Arrows indicate the relative movement
285 of the TRP helix in TRPC3 compared to TRPV1, TRPA1 or TRPM4.

286 **Figure 5: The ion-conducting pore.** (a, d, e) Surface representation of TRPC3, viewed (a)
287 parallel to the membrane, (d) from the extracellular side, and (e) from the intracellular side. The
288 surface is colored according to electrostatic surface potential; the color gradient is from -5 to 5
289 kT/e (red to blue). The protein is also shown in cartoon representation in (a). (b) The shape and
290 size of the ion-conducting pore (boxed area in panel a). The P loop and S6 of two subunits and the
291 TRP helix of the other two subunits are shown as cartoons, and the side chains of restriction
292 residues are shown as sticks. Purple, green, and red spheres define radii of > 2.3, 1.2–2.3, and < 1.2
293 Å, respectively. (c) Plot of pore radius as a function of distance along the pore axis in Angstroms.

294 **Figure 6. The intracellular domain.** (a) Surface representation of TRPC3 with two adjacent
295 subunits shown in cartoon representation. The intracellular domain is highlighted in the black

296 frame. Two interfaces highlighted in green frames are enlarged in (d-e). (b-c) Cartoon
 297 representation of the CTD coiled-coil pole and the rib helix. The intracellular domain is shown in
 298 surface representation, viewed in parallel to the membrane (b) and from the intracellular side (c).
 299 (d) Inter-subunit interface formed by the CTD rib helix with adjacent ARD and LD. Protein is
 300 shown in cartoon and surface representations. Two adjacent subunits are in blue and red. Charged
 301 residues forming hydrogen bond or polar interaction with each other are shown as sticks. (e)
 302 Interface between adjacent LDs and pre-S1. Alpha helices involved in the inter-subunit
 303 interaction are indicated.

304 **Table 1. Statistics of EM data processing and model refinement.**

Data collection/processing	
Microscope	Titan Krios (FEI)
Voltage (kV)	300
Defocus range (μM)	1.0 – 2.5
Exposure time (s)	8
Dose rate ($e^-/\text{\AA}^2/\text{s}$)	6.76
Number of frames	40
Pixel size (\AA)	1.074
Particles refined	143855
Resolution (\AA)	3.3
FSC threshold	0.143
Resolution range (\AA)	412.4 – 3.3
Model statistics	
Number of atoms	20988
Protein	20744
Ligand	244
r.m.s. deviations	
Bond length (\AA)	0.005
Bond angle ($^\circ$)	1.008

Ramachandran plot	
Favored (%)	94.09
Allowed (%)	5.77
Disallowed (%)	0.14
Rotamer outlier (%)	0.85
Clashscore	3.0

305

306 **Figure 1 – figure supplement 1. Preparation, electrophysiological characterization of human**

307 **full-length TRPC3.** (a) Size-exclusion chromatography profile of TRPC3. (b) SDS gel of

308 purified TRPC3. (c) Under whole-cell voltage clamp configuration, HEK-293 cells infected by

309 virus encoding WT TRPC3 receptor gene show robust current when exposing to 10 μ M OAG,

310 this current can be completely blocked by 10 μ M OAG + 100 μ M Pyr3 (n=3 cells).

311 **Figure 1 – figure supplement 2. Cryo-EM analysis of human full-length TRPC3.** (a)

312 Representative electron micrograph. (b) Selected two-dimensional class averages of the electron

313 micrographs. (c) The gold-standard Fourier shell correlation curve for the EM maps is shown in

314 black and the FSC curve between the atomic model and the final EM map is shown in blue. (d)

315 Angular distribution of particles used for refinement.

316 **Figure 1 – figure supplement 3. Cryo-EM map of human full-length TRPC3.** (a-b) Local

317 resolution estimation. The map is colored according to local resolution estimation. (c)

318 Representative densities Density maps are shown in blue meshes, and the atomic models are

319 shown in cartoon representation with side chains as sticks.

320 **Figure 1 – figure supplement 4. Secondary structure arrangement of human TRPC3 and**
321 **sequence alignment of TRPC family channels.** The TRPC2 is from *mus musculus*, whereas all
322 the other proteins are from human. The sequences were aligned using the Clustal Omega
323 program on the Uniprot website and coloured using BLOSUM62 score by conservation. The
324 secondary structural elements are color-coded to match Figure 2a.

325 **Figure 3 – figure supplement 1. Comparison of the TMD of TRPC3 with TRPV1 (a), TRPA1**
326 **(b), and TRPM4 (c).** Structures are aligned using main chain atoms of the pore domain. Only
327 the TMD of one subunit is shown in cartoon representation, viewed in parallel to the membrane.
328 TRPC3 is in blue; TRPV1, TRPA1, and TRPM4 are in pink. (d-e) TMD viewed from
329 extracellular side. The relative organization of the S1-S4 domain with the pore domain in TRPC3
330 is similar to that in TRPV1, but the S1-S4 domain in TRPC3 exhibits a clockwise rotation
331 relative to TRPA1 or TRPM4.

332 **Materials and Methods**

333 **Construct, expression and purification of TRPC3**

334 A full-length human *TRPC3* gene (UniProtKB (<http://www.uniprot.org>) accession number,
335 Q13507) with 836 amino acid residues was synthesized by Genscript and was subcloned into a
336 modified version of pEG BacMam vector containing: a twin strep-tag, a His8-tag, and green
337 fluorescent protein (GFP) with thrombin cleavage site at the N terminus (Goehring et al., 2014).
338 The recombinant Bacmid DNA and baculovirus of TPRC3 were generated by sf9 insect cells,
339 and P2 viruses were used to infect suspension HEK293 cells. The recombinant Bacmid DNA and

340 baculovirus of TRPC3 were generated by sf9 insect cells, and P2 viruses were used to infect
341 suspension HEK293 cells. The HEK293 and sf9 were obtained from the ATCC and were not
342 re-authenticated or tested for mycoplasma after purchase.

343

344 For large-scale expression, suspension HEK293 cells were cultured in Freestyle 293
345 expression Medium (Invitrogen) with 1% (v/v) fetal bovine serum (FBS). When cell density
346 reached around 3 million/ml, 8% (v/v) of P2 viruses were introduced. At 12 h post-infection, 10
347 mM sodium butyrate was supplemented and then cells were transferred to 30 °C. The infected
348 cells were collected at 48 h post-infection by centrifugation at 4000 rpm for 15 min at 4 °C and
349 then was washed once with TBS buffer (20 mM Tris, pH 8.0, 150 mM NaCl).

350 TRPC3 was extracted from the cells by solubilization buffer containing 20 mM Tris 8.0,
351 500 mM NaCl in the presence of 1 mM PMSF, 0.8 μM aprotinin, 2 μg/ml leupeptin, and 2 mM
352 pepstatin A with 1% digitonin (Calbiochem) for 2 h at 4 °C. The cell debris were eradicated by
353 ultracentrifugation at 40,000 rpm using 45 Ti rotor (Beckman Coulter, Inc.) for 1 h at 4 °C. The
354 solubilized proteins were incubated with TALON resin and the resin was washed with 10 column
355 volumes of wash buffer (20 mM Tris 8.0, 500 mM NaCl, 15 mM imidazole, and 0.1% digitonin).
356 The TALON resin-bound TRPC3 was eluted with elution buffer (20 mM Tris 8.0, 500 mM NaCl,
357 250 mM imidazole, and 0.1% digitonin). Thrombin (1:20 molar ratio) and 10 mM EDTA were
358 added into the eluted sample and incubated for 3 h on the ice. In order to further purify the
359 protein, the sample was concentrated and loaded onto a superpose6 column in buffer containing

360 20 mM Tris 8.0, 500 mM NaCl, 1 mM EDTA with 0.1% digitonin. Peak fractions containing
361 TRPC3 were pooled and concentrated to 5 mg/ml.

362 **EM sample preparation and data acquisition**

363 The purified TRPC3 protein sample (2.5 μ L) at a concentration of 5 mg/mL was applied onto a
364 glow-discharged Quantifoil holey carbon grid (gold, 1.2/1.3 μ m size/hole space, 300 mesh). The
365 grid was blotted for 1.5 s at 100% humidity by using a Vitrobot Mark III, and then was plunged
366 into liquid ethane cooled by liquid nitrogen. Images were obtained by an FEI Titan Krios
367 electron microscope operating at 300 kV with a nominal magnification of 130,000 \times Gatan K2
368 Summit direct electron detector was used in order to record image stacks in super-resolution
369 counting mode with a binned pixel size of 1.074 \AA . Every image was dose-fractionated to 40
370 frames with a total exposure time of 8 s with 0.2 s per frame. Dose rate was 6.76 $e^- \text{\AA}^{-2} s^{-1}$. The
371 images stacks were recorded using the automated acquisition program SerialEM (Mastronarde,
372 2005). Nominal defocus values varied from 1.0 to 2.5 μ m.

373 **EM data processing**

374 MotionCor2 was used to implement motion-correction of summed movie stacks(Zheng et al.,
375 2017). Gctf was applied to estimate Defocuse values (Zhang, 2016). Particles were picked from
376 approximately 200 micrographs using Gautomatch
377 (<http://www.mrc-lmb.cam.ac.uk/kzhang/Gautomatch/>) and subjected to an initial reference-free
378 2D classification using Relion 2.1(Scheres, 2012). Nine representative 2D class averages were
379 selected as templates for automated particle picking for the entire data set using Gautomatch. The

380 auto-picked particles were visually checked and obvious bad particles were manually removed.
381 The picked particles were cleaned up throughout three rounds of 2D classification. CryoSPARC
382 was applied to obtain an initial model (Punjani et al., 2017). The selected particles after 2D
383 classification were subjected to 3D classification of 5 classes using Relion 2.1, with the initial
384 reconstruction low-pass-filtered to 60 Å as a reference model. Only one out of five classes
385 presented high-resolution features, hence, particles from this class were combined and further
386 refined via Relion 2.1. Particles were further refined using the local refinement from FREALIGN
387 with C4 symmetry applied and high-resolution limit for particle alignment set to 4.5 Å (Grigorieff,
388 2016). The resolutions reported are based on the “limiting resolution” procedure in which the
389 resolution during refinement is limited to a lower resolution than the resolution estimated for the
390 final reconstruction. The final resolutions reported in Table 1 are based on the gold standard
391 Fourier shell correlation (FSC) 0.143 criteria. To calculate the FSC plot, a soft mask (4.3 Å
392 extended from the reconstruction with an additional 4.3 Å cosine soft edge, low-pass filtered to
393 10 Å) was applied to the two half maps.

394 **Model building**

395 The model of TRPC3 was built in Coot using the TMD domain of TRPM4 structure (PDB 5wp6)
396 as a guide (Emsley et al., 2010). *De novo* building was mainly guided by bulky residues and
397 secondary structure prediction (Figure 1-Figure supplement 4). The TRPC3 structure chiefly
398 consists of α helices, which greatly assisted register assignment. In the initial *de novo*-built
399 model, the order and length of the secondary structure features, as well as the positions of bulky

400 residues within each secondary structure feature are in good agreement with the prediction
401 (Figure 1-Figure supplement 4). The initial model was then subjected to real space refinement
402 using Phenix.real_space_refine with secondary structure restraints (Afonine et al., 2012). The
403 refined model was manually examined and re-modified via COOT. For validation of refined
404 structure, FSC curves were applied to calculate the difference between the final model and EM
405 map. The geometries of the atomic models were evaluated using MolProbity (Chen et al., 2010).
406 All figures were prepared using UCSF Chimera and Pymol (Schrödinger) (The PyMOL
407 Molecular Graphics System) (Pettersen et al., 2004).

408 **Electrophysiology**

409 Suspension HEK293 cells were cultured in Freestyle 293 expression Medium (Invitrogen) with
410 1% (v/v) fetal bovine serum (FBS). When cell density reached around 1 million/ml, 5% (v/v) of
411 P2 viruses of human TRPC3 were introduced. Infected cells were incubated in 24-well plate at
412 37 °C, and were recorded 12–24h post-infection. Whole-cell voltage clamp recordings were
413 performed using a HEKA EPC-10 amplifier at room temperature. The holding potential was
414 +60mV. The electrodes were filled with internal solution containing (mM) 130 CsOH, 130
415 glutamate, 3.1 MgCl₂, 2.8 CaCl₂, 10 EGTA, 2 ATPNa₂, 0.3 GTPNa₂, 10 HEPES (pH 7.2 adjusted
416 with CsOH). The bath solution contains (mM) 140 NaCl, 5 KCl, 2 CaCl₂, 1 MgCl₂, 10 glucose,
417 10 HEPES (pH 7.4 adjusted with NaOH). Solution change was done using a two-barrel
418 theta-glass pipette controlled manually. Data were acquired at 10 kHz using Patchmaster
419 software (HEKA). Data were filtered at 1 kHz, and analyzed with Axograph software

420 (www.axograph.com).

421 **Data Availability**

422 The cryo-EM density map and coordinate of TRPC3 have been deposited in the Electron
423 Microscopy Data Bank (EMDB) accession number EMD-7620, and in the RCSB Protein Data
424 Bank (PDB) accession code 6CUD.

425 **Acknowledgements**

426 We thank G. Zhao and X. Meng for the support with data collection at the David Van Andel
427 Advanced Cryo-Electron Microscopy Suite. We appreciate the VARI High-Performance
428 Computing team for computational support. We thank D. Nadziejka for technical editing, and
429 C-H. Lee for helpful discussion. This work was supported by internal VARI funding.

430

431 **References**

432 Afonine, P.V., Grosse-Kunstleve, R.W., Echols, N., Headd, J.J., Moriarty, N.W., Mustyakimov, M., Terwilliger, T.C.,
433 Urzhumtsev, A., Zwart, P.H., and Adams, P.D. (2012). Towards automated crystallographic structure refinement with
434 phenix.refine. *Acta Crystallogr D* **68**, 352-367.

435 Autzen, H.E., Myasnikov, A.G., Campbell, M.G., Asarnow, D., Julius, D., and Cheng, Y.F. (2018). Structure of the
436 human TRPM4 ion channel in a lipid nanodisc. *Science* **359**, 228-232.

437 Beck, A., Speicher, T., Stoerger, C., Sell, T., Dettmer, V., Jusoh, S.A., Abdulmughni, A., Cavalie, A., Philipp, S.E., Zhu,
438 M.X., *et al.* (2013). Conserved Gating Elements in TRPC4 and TRPC5 Channels. *J Biol Chem* **288**, 19471-19483.

439 Becker, E.B.E. (2014). The Moonwalker Mouse: New Insights into TRPC3 Function, Cerebellar Development, and
440 Ataxia. *Cerebellum* **13**, 628-636.

441 Becker, E.B.E., Fogel, B.L., Rajakulendran, S., Dulneva, A., Hanna, M.G., Perlman, S.L., Geschwind, D.H., and Davies,
442 K.E. (2011). Candidate Screening of the TRPC3 Gene in Cerebellar Ataxia. *Cerebellum* **10**, 296-299.

443 Berridge, M.J., Bootman, M.D., and Roderick, H.L. (2003). Calcium signalling: Dynamics, homeostasis and
444 remodelling. *Nat Rev Mol Cell Bio* **4**, 517-529.

445 Chen, V.B., Arendall, W.B., Headd, J.J., Keedy, D.A., Immormino, R.M., Kapral, G.J., Murray, L.W., Richardson, J.S.,
446 and Richardson, D.C. (2010). MolProbity: all-atom structure validation for macromolecular crystallography. *Acta*

447 Crystallogr D 66, 12-21.

448 Dietrich, A., Schnitzler, M.M.Y., Emmel, J., Kalwa, H., Hofmann, T., and Gudermann, T. (2003). N-linked protein
449 glycosylation is a major determinant for basal TRPC3 and TRPC6 channel activity. *J Biol Chem* 278, 47842-47852.

450 Emsley, P., Lohkamp, B., Scott, W.G., and Cowtan, K. (2010). Features and development of Coot. *Acta Crystallogr D*
451 66, 486-501.

452 Fogel, B., Hanson, S., and Becker, E. (2016). Mutation of the Murine Ataxia Gene TRPC3 Causes Cerebellar Ataxia in
453 Humans. *Neurology* 86, 284-286.

454 Garcia-Martinez, C., Morenilla-Palao, C., Planells-Cases, R., Merino, J.M., and Ferrer-Montiel, A. (2000).
455 Identification of an aspartic residue in the P-loop of the vanilloid receptor that modulates pore properties. *J Biol*
456 *Chem* 275, 32552-32558.

457 Garcia-Sanz, N., Valente, P., Gomis, A., Fernandez-Carvajal, A., Fernandez-Ballester, G., Viana, F., Belmonte, C., and
458 Ferrer-Montiel, A. (2007). A role of the transient receptor potential domain of vanilloid receptor I in channel Gating.
459 *J Neurosci* 27, 11641-11650.

460 Goehring, A., Lee, C.H., Wang, K.H., Michel, J.C., Claxton, D.P., Bacongus, I., Althoff, T., Fischer, S., Garcia, K.C., and
461 Gouaux, E. (2014). Screening and large-scale expression of membrane proteins in mammalian cells for structural
462 studies. *Nat Protoc* 9, 2574-2585.

463 Gonzalez-Cobos, J.C., and Trebak, M. (2010). TRPC channels in smooth muscle cells. *Front Biosci-Landmrk* 15,
464 1023-1039.

465 Gregorio-Teruel, L., Valente, P., Gonzalez-Ros, J.M., Fernandez-Ballester, G., and Ferrer-Montiel, A. (2014). Mutation
466 of I696 and W697 in the TRP box of vanilloid receptor subtype I modulates allosteric channel activation. *J Gen*
467 *Physiol* 143, 361-375.

468 Grigorieff, N. (2016). FREALIGN: An Exploratory Tool for Single-Particle Cryo-EM. *Methods Enzymol* 579, 191-226.

469 Guo, J.T., She, J., Zeng, W.Z., Chen, Q.F., Bai, X.C., and Jiang, Y.X. (2017). Structures of the calcium-activated,
470 non-selective cation channel TRPM4. *Nature* 552, 205-209.

471 Itsuki, K., Imai, Y., Okamura, Y., Abe, K., Inoue, R., and Mori, M.X. (2012). Voltage-sensing phosphatase reveals
472 temporal regulation of TRPC3/C6/C7 channels by membrane phosphoinositides. *Channels* 6, 206-209.

473 Jin, P., Bulkley, D., Guo, Y.M., Zhang, W., Guo, Z.H., Huynh, W., Wu, S.P., Meltzer, S., Cheng, T., Jan, L.Y., *et al.* (2017).
474 Electron cryo-microscopy structure of the mechanotransduction channel NOMPC. *Nature* 547, 118-122.

475 Kitajima, N., Numaga-Tomita, T., Watanabe, M., Kuroda, T., Nishimura, A., Miyano, K., Yasuda, S., Kuwahara, K., Sato,
476 Y., Ide, T., *et al.* (2016). TRPC3 positively regulates reactive oxygen species driving maladaptive cardiac remodeling.
477 *Sci Rep-Uk* 6, 1-14.

478 Kiyonaka, S., Kato, K., Nishida, M., Mio, K., Numaga, T., Sawaguchi, Y., Yoshida, T., Wakamori, M., Mori, E., Numata,
479 T., *et al.* (2009). Selective and direct inhibition of TRPC3 channels underlies biological activities of a pyrazole
480 compound. *P Natl Acad Sci USA* 106, 5400-5405.

481 Kumar, R., and Thompson, J.R. (2011). The Regulation of Parathyroid Hormone Secretion and Synthesis. *J Am Soc*
482 *Nephrol* 22, 216-224.

483 Li, H.S., Xu, X.Z.S., and Montell, C. (1999). Activation of a TRPC3-dependent cation current through the
484 neurotrophin BDNF. *Neuron* 24, 261-273.

485 Lichtenegger, M., Stockner, T., Poteser, M., Schleifer, H., Platzer, D., Romanin, C., and Groschner, K. (2013). A novel
486 homology model of TRPC3 reveals allosteric coupling between gate and selectivity filter. *Cell Calcium* 54, 175-185.

487 Lichtenegger, M., Tiapko, O., Svobodova, B., Stockner, T., Glasnov, T.N., Schreibmayer, W., Platzer, D., de la Cruz, G.G.,

488 Krenn, S., Schober, R., *et al.* (2018). An optically controlled probe identifies lipid-gating fenestrations within the
489 TRPC3 channel. *Nat Chem Biol*.

490 Liu, X.B., Singh, B.B., and Ambudkar, I.S. (2003). TRPC1 is required for functional store-operated Ca²⁺ channels -
491 Role of acidic amino acid residues in the S5-S6 region. *J Biol Chem* 278, 11337-11343.

492 Long, S.B., Tao, X., Campbell, E.B., and MacKinnon, R. (2007). Atomic structure of a voltage-dependent K⁺ channel
493 in a lipid membrane-like environment. *Nature* 450, 376-382.

494 Mastrorarde, D.N. (2005). Automated electron microscope tomography using robust prediction of specimen
495 movements. *J Struct Biol* 152, 36-51.

496 Ni, C., Yan, M., Zhang, J., Cheng, R.H., Liang, J.Y., Deng, D., Wang, Z., Li, M., and Yao, Z. (2016). A novel mutation in
497 TRPV3 gene causes atypical familial Olmsted syndrome. *Sci Rep-Uk* 6, 1-10.

498 Nilius, B., Prenen, J., Janssens, A., Owsianik, G., Wang, C.B., Zhu, M.X., and Voets, T. (2005a). The selectivity filter of
499 the cation channel TRPM4. *J Biol Chem* 280, 22899-22906.

500 Nilius, B., Talavera, K., Owsianik, G., Prenen, J., Droogmans, G., and Voets, T. (2005b). Gating of TRP channels: a
501 voltage connection? *J Physiol-London* 567, 35-44.

502 Oda, K., Umemura, M., Nakakaji, R., Tanaka, R., Sato, I., Nagasako, A., Oyamada, C., Baljinnnyam, E., Katsumata, M.,
503 Xie, L.H., *et al.* (2017). Transient receptor potential cation 3 channel regulates melanoma proliferation and
504 migration. *J Physiol Sci* 67, 497-505.

505 Ong, H.L., de Souza, L.B., and Ambudkar, I.S. (2016). Role of TRPC Channels in Store-Operated Calcium Entry. *Adv*
506 *Exp Med Biol* 898, 87-109.

507 Paulsen, C.E., Armache, J.P., Gao, Y., Cheng, Y.F., and Julius, D. (2016). Structure of the TRPA1 Ion Channel Suggests
508 Regulatory Mechanisms. *Biophys J* 110, 26a-26a.

509 Pettersen, E.F., Goddard, T.D., Huang, C.C., Couch, G.S., Greenblatt, D.M., Meng, E.C., and Ferrin, T.E. (2004). UCSF
510 chimera - A visualization system for exploratory research and analysis. *J Comput Chem* 25, 1605-1612.

511 Poteser, M., Schleifer, H., Lichtenegger, M., Schernthaner, M., Stockner, T., Kappe, C.O., Glasnov, T.N., Romanin, C.,
512 and Groschner, K. (2011). PKC-dependent coupling of calcium permeation through transient receptor potential
513 canonical 3 (TRPC3) to calcineurin signaling in HL-1 myocytes. *Proc Natl Acad Sci U S A* 108, 10556-10561.

514 Prakriya, M., and Lewis, R.S. (2015). Store-Operated Calcium Channels. *Physiol Rev* 95, 1383-1436.

515 Punjani, A., Rubinstein, J.L., Fleet, D.J., and Brubaker, M.A. (2017). cryoSPARC: algorithms for rapid unsupervised
516 cryo-EM structure determination. *Nat Methods* 14, 290-296.

517 Scheres, S.H.W. (2012). RELION: Implementation of a Bayesian approach to cryo-EM structure determination. *J*
518 *Struct Biol* 180, 519-530.

519 Shen, P.S., Yang, X.Y., DeCaen, P.G., Liu, X.W., Bulkley, D., Clapham, D.E., and Cao, E.H. (2016). The Structure of the
520 Polycystic Kidney Disease Channel PKD2 in Lipid Nanodiscs. *Cell* 167, 763-773.

521 Smyth, J.T., Hwang, S.Y., Tomita, T., DeHaven, W.I., Mercer, J.C., and Putney, J.W. (2010). Activation and regulation of
522 store-operated calcium entry. *J Cell Mol Med* 14, 2337-2349.

523 Strubing, C., Krapivinsky, G., Krapivinsky, L., and Clapham, D.E. (2003). Formation of novel TRPC channels by
524 complex subunit interactions in embryonic brain. *J Biol Chem* 278, 39014-39019.

525 Sudhof, T.C. (2012). Calcium Control of Neurotransmitter Release. *Csh Perspect Biol* 4.

526 Taberner, F.J., Lopez-Cordoba, A., Fernandez-Ballester, G., Korchev, Y., and Ferrer-Montiel, A. (2013). Mutations in
527 the TRP Domain Differentially affect the Function of TRPM8. *Biophys J* 104, 456a-456a.

528 Tang, J., Lin, Y.K., Zhang, Z.M., Tikunova, S., Birnbaumer, L., and Zhu, M.X. (2001). Identification of common binding

529 sites for calmodulin and inositol 1,4,5-trisphosphate receptors on the carboxyl termini of Trp channels. *J Biol Chem*
530 *276*, 21303-21310.

531 Vannier, B., Zhu, X., Brown, D., and Birnbaumer, L. (1998). The membrane topology of human transient receptor
532 potential 3 as inferred from glycosylation-scanning mutagenesis and epitope immunocytochemistry. *J Biol Chem*
533 *273*, 8675-8679.

534 Vazquez, G., Wedel, B.J., Aziz, O., Trebak, M., and Putney, J.W. (2004). The mammalian TRPC cation channels.
535 *Bba-Mol Cell Res* *1742*, 21-36.

536 Winkler, P.A., Huang, Y.H., Sun, W.N., Du, J., and Lu, W. (2017). Electron cryo-microscopy structure of a human
537 TRPM4 channel. *Nature* *552*, 200-204.

538 Xia, M., Liu, D., and Yao, C. (2015). TRPC3: A New Target for Therapeutic Strategies in Chronic Pain - DAG-mediated
539 Activation of Non-selective Cation Currents and Chronic Pain. *J Neurogastroenterol* *21*, 445-447.

540 Yang, S.L., Cao, Q., Zhou, K.C., Feng, Y.J., and Wang, Y.Z. (2009). Transient receptor potential channel C3 contributes
541 to the progression of human ovarian cancer. *Oncogene* *28*, 1320-1328.

542 Yin, Y., Wu, M.Y., Zubcevic, L., Borschel, W.F., Lander, G.C., and Lee, S.Y. (2018). Structure of the cold- and
543 menthol-sensing ion channel TRPM8. *Science* *359*, 237-241.

544 Zhang, K. (2016). Gctf: Real-time CTF determination and correction. *J Struct Biol* *193*, 1-12.

545 Zheng, S.Q., Palovcak, E., Armache, J.P., Verba, K.A., Cheng, Y.F., and Agard, D.A. (2017). MotionCor2: anisotropic
546 correction of beam-induced motion for improved cryo-electron microscopy. *Nat Methods* *14*, 331-332.

547 Zhu, X., Jiang, M.S., and Birnbaumer, L. (1998). Receptor-activated Ca²⁺ influx via human Trp3 stably expressed in
548 human embryonic kidney (HEK)293 cells - Evidence for a non-capacitative Ca²⁺ entry. *J Biol Chem* *273*, 133-142.

549 Zhu, X., Jiang, M.S., Peyton, M., Boulay, G., Hurst, R., Stefani, E., and Birnbaumer, L. (1996). trp, a novel mammalian
550 gene family essential for agonist-activated capacitative Ca²⁺ entry. *Cell* *85*, 661-671.

551

552

Figure 1

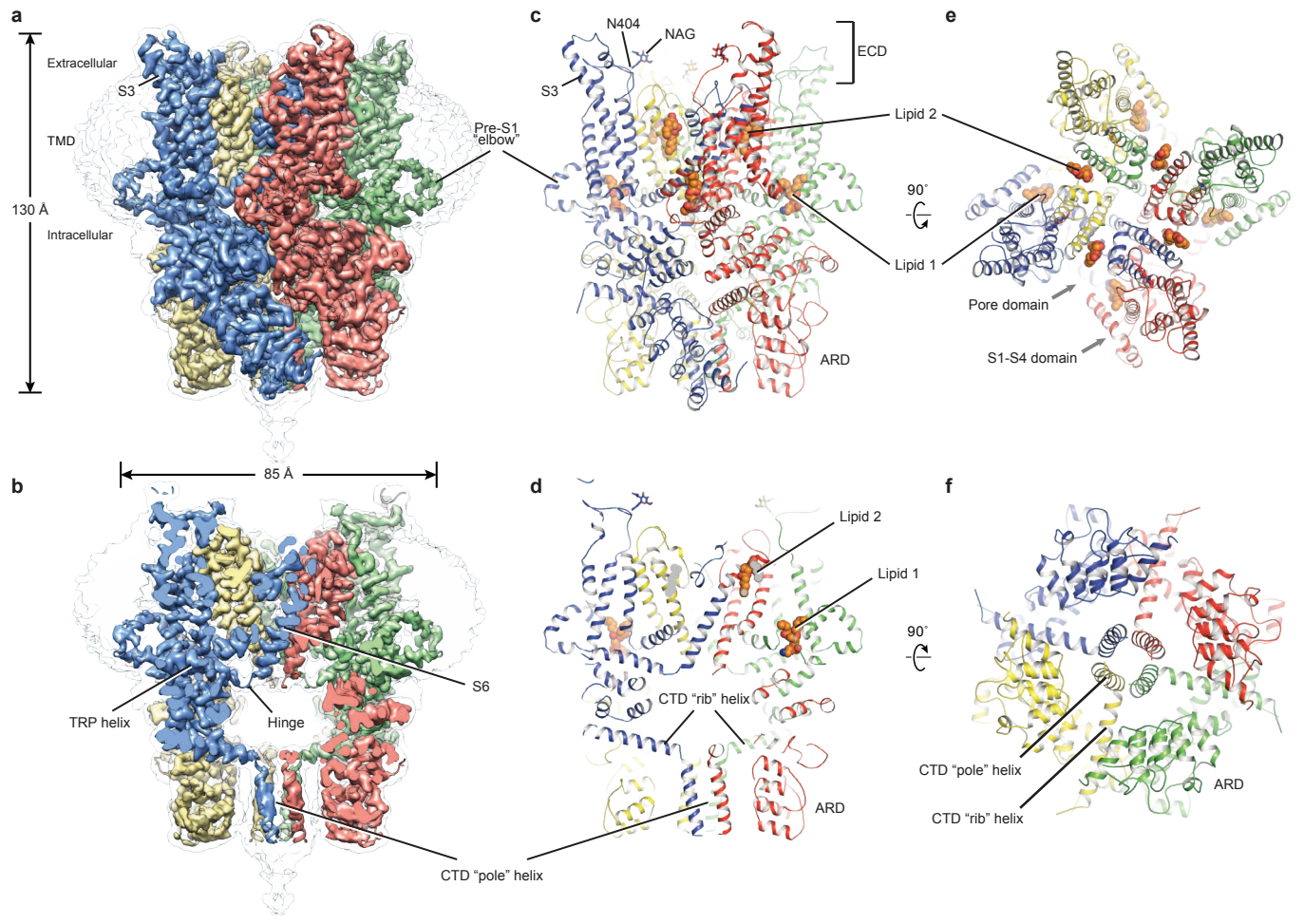


Figure 2

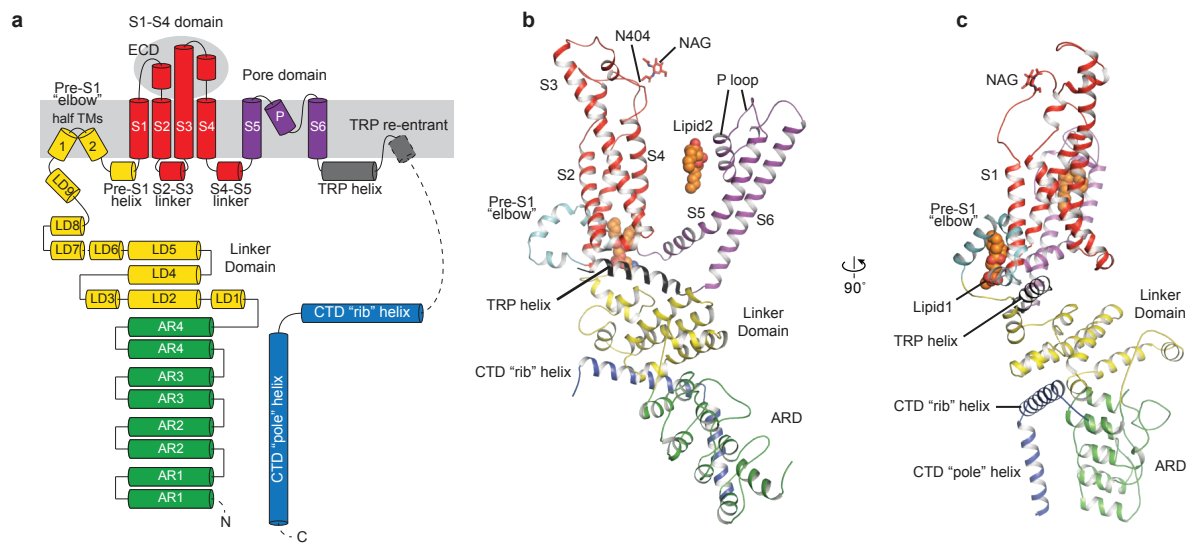


Figure 3

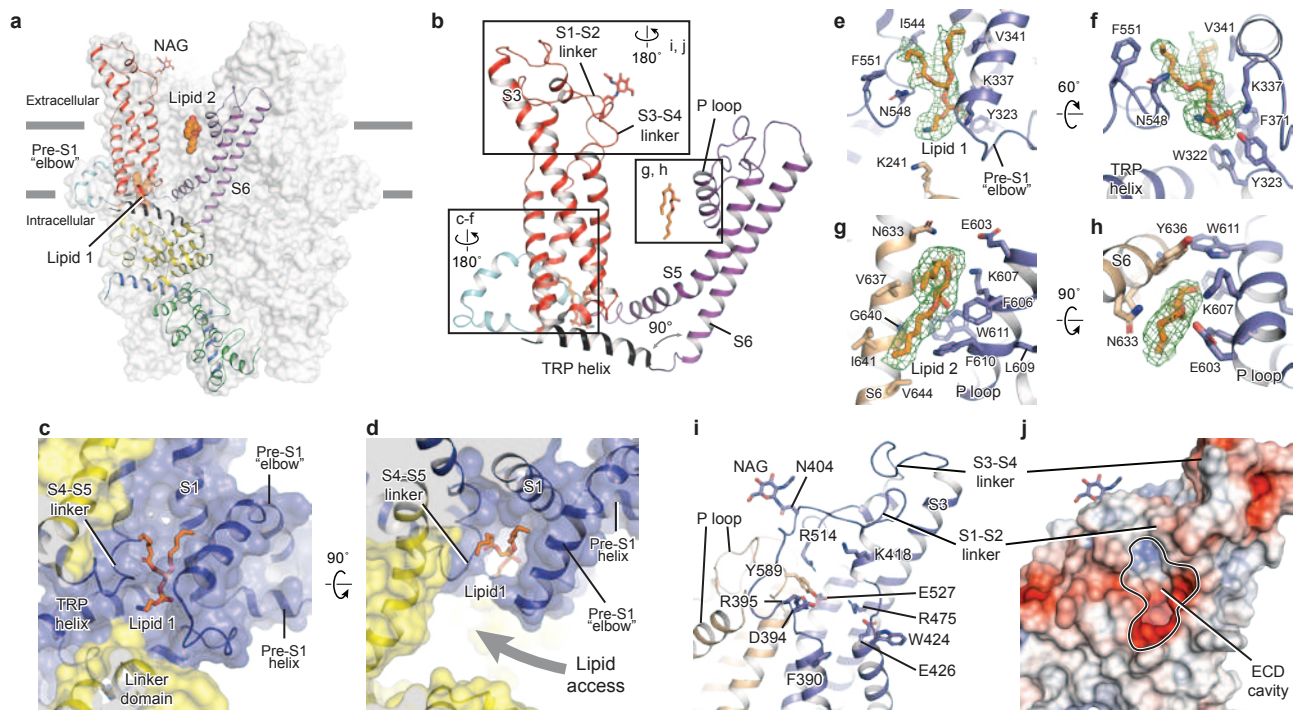


Figure 4

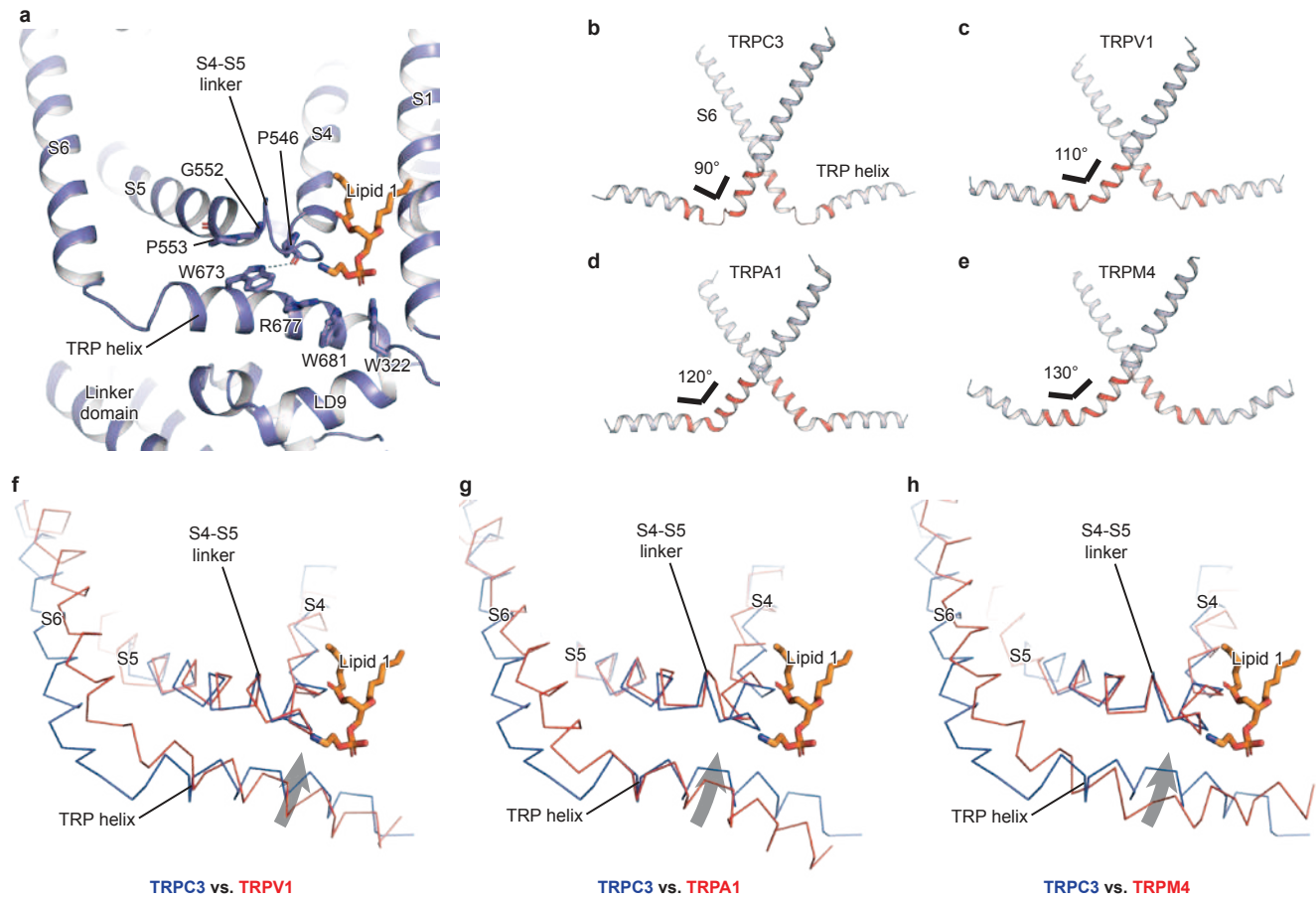


Figure 5

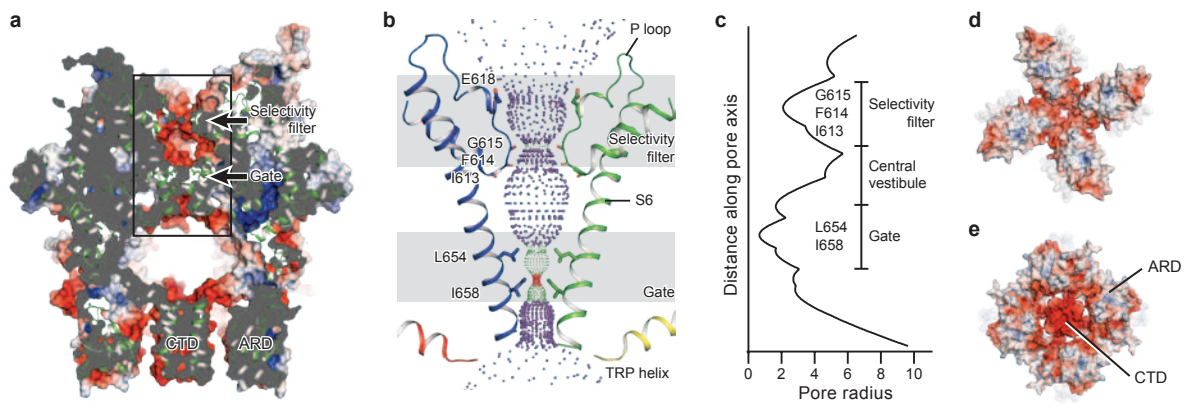


Figure 6

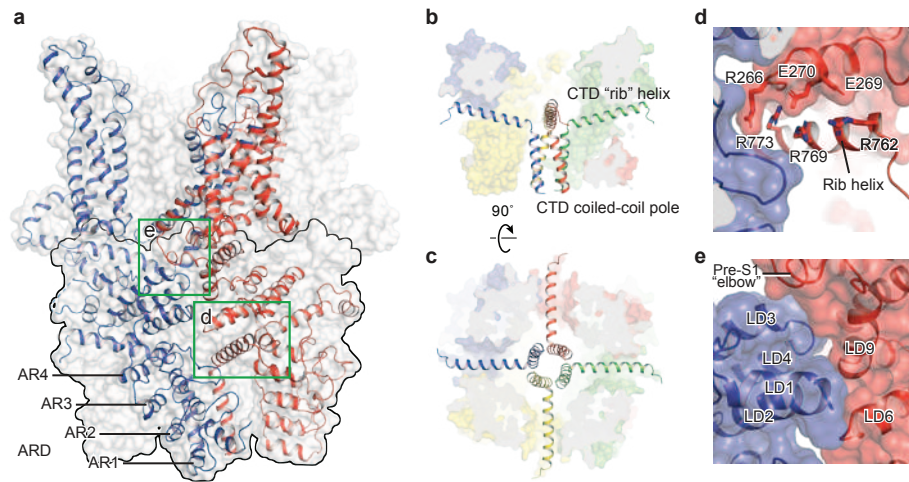


Figure 1 – figure supplement 1

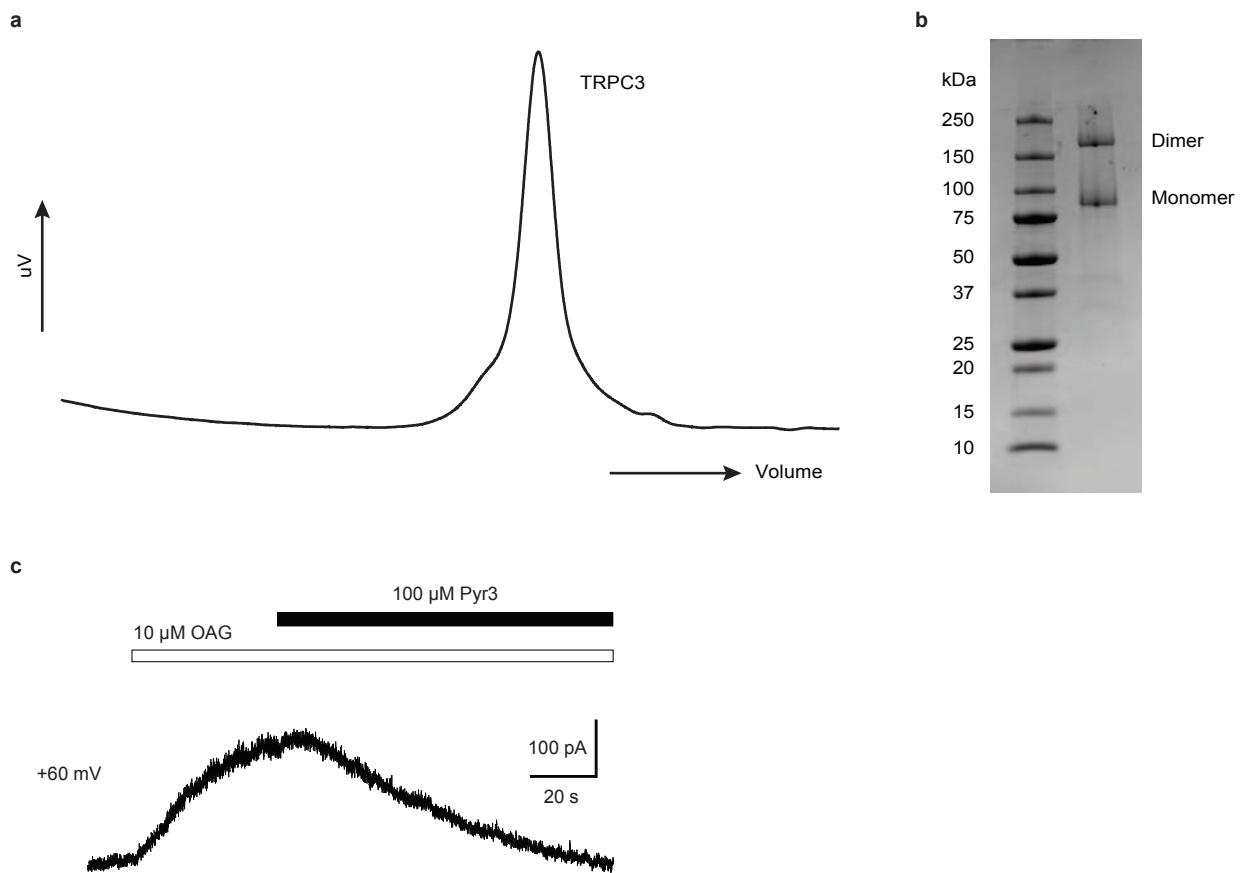


Figure 1 – figure supplement 2

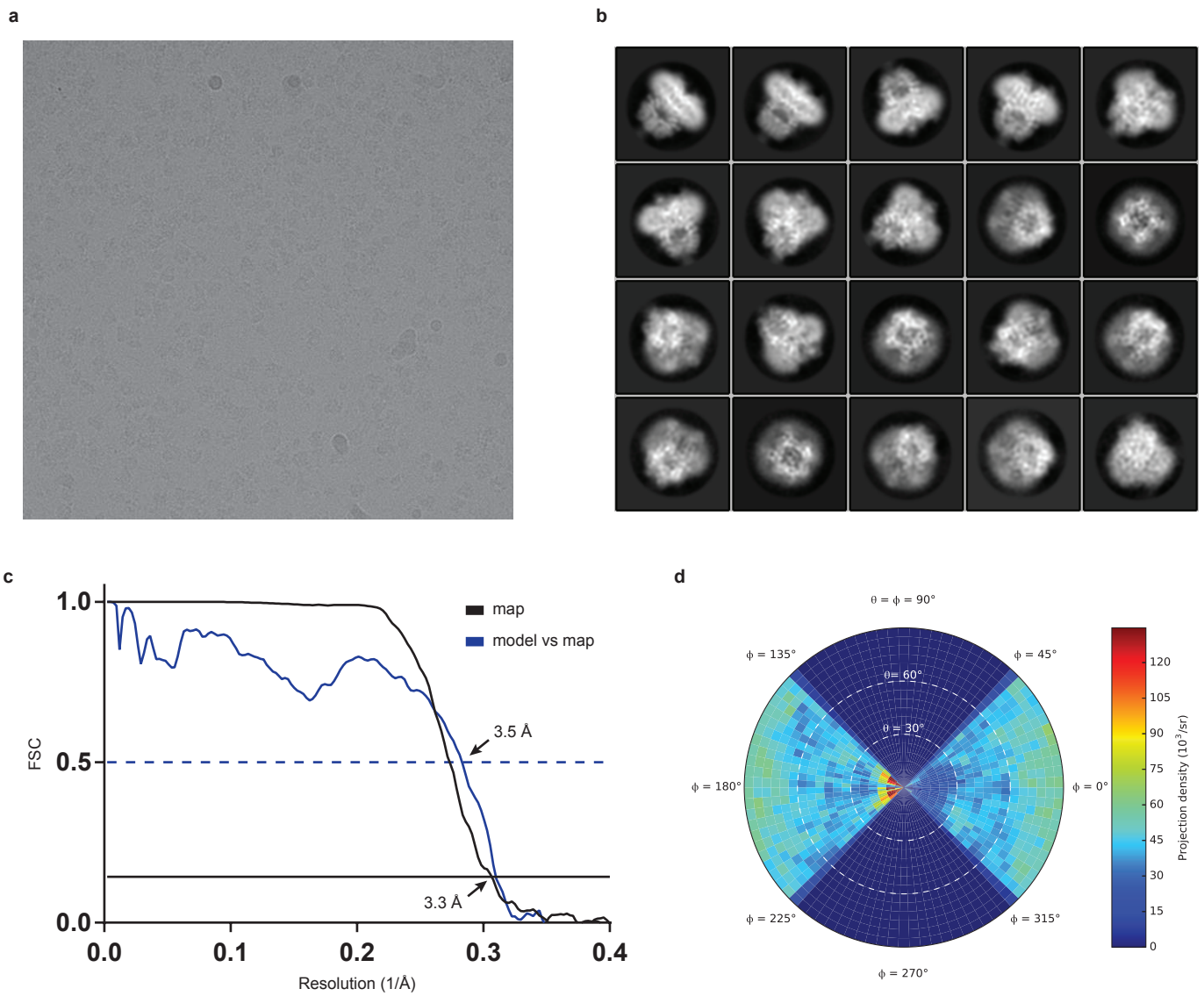


Figure 1 – figure supplement 3

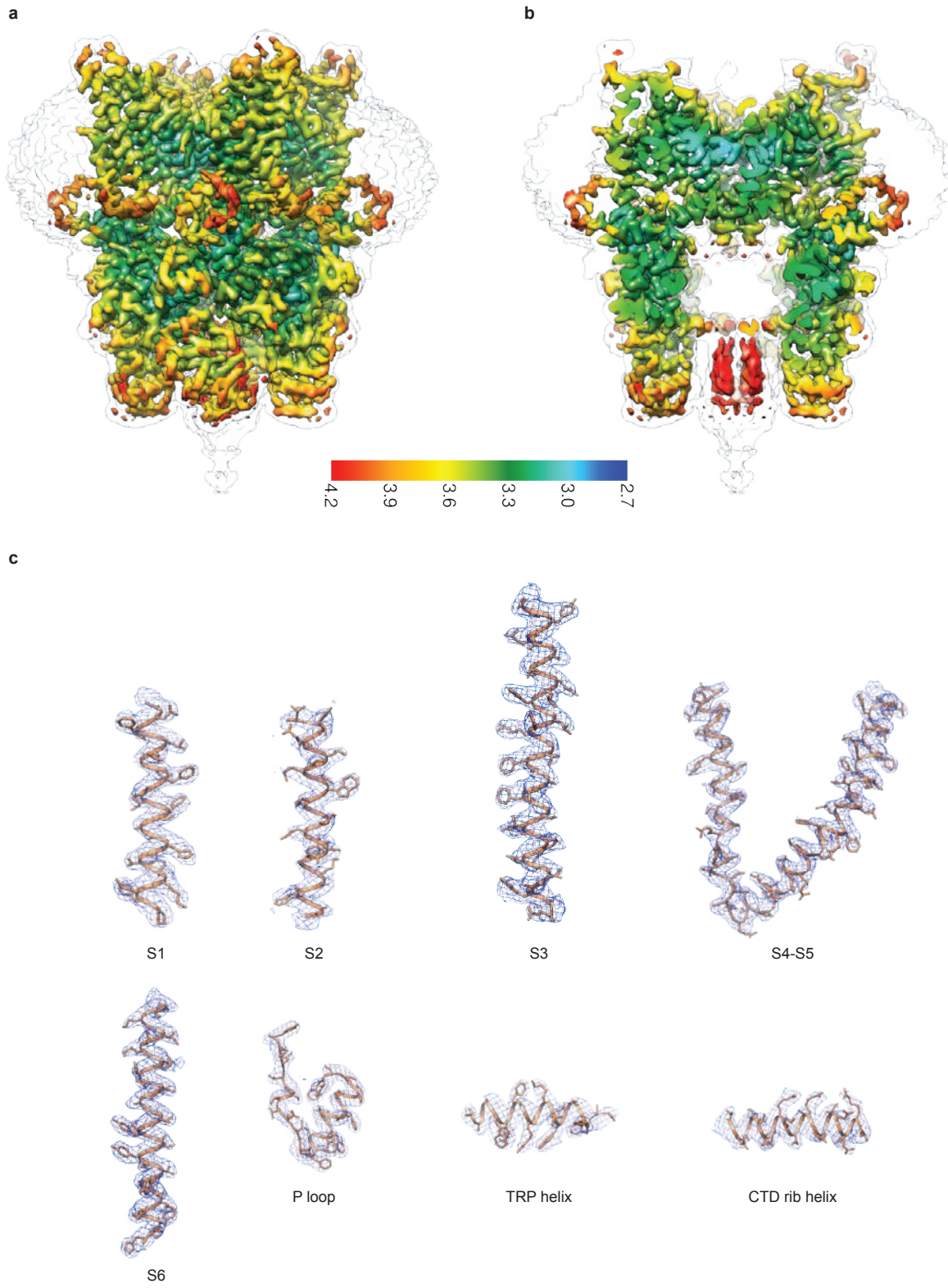


Figure 1 – figure supplement 4

Human_TRPC3	1	-----MREKGRQAVRGPAFMFDNRGTSLTAEERFLDAAEYGNIPVVRKMLEE	49
Human_TRPC6	56	CFRGS-----DNRLAHRRTVLRKGRRLANRGPAYMFSDRSLSLSEERFLDAAEYGNIPVVRKMLEE	120
Human_TRPC7	1	MLRNS-----TFKNMQRHTTLREKGRRAIRGPAYMFNEKGTSLTPEEERFLDAAEYGNIPVVRKMLEE	65
Human_TRPC1	8	STDLS-----GASSSSLPSSPSSSSPN-----EVMALKDVRVKEENTLNEKFLFLLACDKGDIYVMVKILEE	69
Human_TRPC4	7	KRNVN-----APYRD-----RIPLRIVRAEELSPSEKAYLNAVEKGDYASVKKILEE	54
Human_TRPC5	7	KVNVY-----SPYRD-----RIPLQIVRAEELSAEKAFLNAVEKGDYATVKALQE	54
Mouse_TRPC2	241	IETLPQHAATCGESPQPASPASLSSESVLRRHVHALTPV-PL--VPKQPWNTEIVNKKLKFPPTLRRAIQEGQLGLVQQLLES	324
Human_TRPC3	50	SK---TLNVN-----CVDYMGQNALQLAVGNEHLEVTELLK--KENLARIGDALLLAISKGYVRIVEAILNHPGFAASKR	120
Human_TRPC6	121	CH---SLNVN-----CVDYMGQNALQLAVANEHLEITELLK--KENLSRVGDALLLAISKGYVRIVEAILNSHPAFAEGKR	191
Human_TRPC7	66	SK---TLNFN-----CVDYMGQNALQLAVGNEHLEVTELLK--KENLARVGDALLLAISKGYVRIVEAILNHPAFAQQGR	136
Human_TRPC1	70	NS-SGDLNIN-----CVDVLRNVAITITENENLDLQLLLDY---GCQSADALLVAIDSEVVGAVDILLNHRPKRSSRP	140
Human_TRPC4	55	AEIYFKININ-----CIDPLGRRTALLIAIENENLELIELLSF---NVYVGDALLHAIRKEVVGAVELLLNKKPSGEKQ	126
Human_TRPC5	55	AEIYVNVNIN-----CMDPLGRSALLIAIENENLEIMELLNHN---SVYVGDALLYAIRKEVVGAVELLLSYRRPSGEKQ	126
Mouse_TRPC2	325	SS---DASGAGGGPLRNVEESEDRSWREALNLAIRLGVHETDVLINLVANVKFDFRQIHEALLVAVDTNQPAVVRLLARLERKGRK	408
Human_TRPC3	121	LTLSPCQEQLQDDDFYAYDEGTRFSPDITPIILAAHCQYEVVHMLLMKGARIERPHDYFCCKGDCMEKQRHDSFHSRSRINAYK	207
Human_TRPC6	192	LATSPSQSELQDDDFYAYDEGTRFSDVTPPIILAAHCQYEVIVHTLLRKGARIERPHDYFCCKNDNCQKQKHSFHSRSRINAYK	278
Human_TRPC7	137	LTLSPLLEQLRDDDFYAYDEGTRFSDITPIILAAHCQYEVIVHLLKKGARIERPHDYFCCKNECTEKQRKDSFHSRSRINAYK	223
Human_TRPC1	141	TIVKLM-----RIQNPEYSTTMDVAPVILAAHRNNEYILTMLLKQVSLPKPHAVGCECTLCSAKNKHDSFHSRSRINAYK	218
Human_TRPC4	127	VPP-I LL-----DKQFS---EFTPDITPIILAAHTNNEYIKLLVQKGVSPRPHEVRCNCEVCSSSDVSRLHRSRRLNIYK	201
Human_TRPC5	127	VPT-LMM-----DTQFS---EFTPDITPIIMLAHTNNEYIKLLVQKGVTPRPHQIRCNCEVCSSEVSDSLHRSRRLNIYK	201
Mouse_TRPC2	409	VD-----TKSFLAFDSSIDGSRFAPGVPTTLACQKHLVEIAQLLMDQKVTIARPHVSCALECSNARRYDLLKFLSRLINTYK	490
Human_TRPC3	208	GLASPAYLSLSEDPVLTALLESNELAKLANIEKEFKNDYKLSMCKDFVVGVLDCRDSEEVVEAILNGDLESAEP-----LE	286
Human_TRPC6	279	GLASPAYLSLSEDPVMTALELSNELAVLANIEKEFKNDYKLSMCKDFVVGVLDCRNTTEEVEAILNGDVFLQ-----S	355
Human_TRPC7	224	GLASAAVLSLSEDPVLTALLESNELAKLANIEEKFNDYKLSMCKDFVVGVLDCRDTEVEAILNGDVNFVQ-----W	300
Human_TRPC1	219	CLASPALIMLTEDDPILRAFELSADLKELSVEEFRNDYELARQCKMFAKDLAQARNRSRELEVINHTSSDEPLD-----KW	299
Human_TRPC4	202	ALASPSLIALESDEPFLTAFQLSWEQLSKVNEFKSEYELSRQCKQKAKDLDDQTRSSRELEIILNRRDSDNSL-I-----	278
Human_TRPC5	202	ALASPSLIALESDEPILTAFRLGWLELKSVEFKAEYELSSQCKLFAKDLDDQARSRELEIILNHRDDHSEEL-----	279
Mouse_TRPC2	491	GLASRAHLSLASEDAMLAFLSRELRRLARKEPEFKPQYIALESICQDYGFELGMCNRQSEPTAVLNDLGEDSETEPEAEGLGA	577
Human_TRPC3	287	VHRHKASLSRVKLAIKYEVKFFVAHPNCQQQLTIWYENLSGLREQTIAIKCLVVLVVALGLPFLAIGYWIAPCSRIGKILRSPFMK	373
Human_TRPC6	356	GDHGRPNLSRLKLAIKYEVKFFVAHPNCQQQLLSIWYENLSGLRQQTMAVFLVVALVAVIIGLFLALIIYWFAPCSKMGKIMRGPFMK	442
Human_TRPC7	301	SDHHRPSSLRIKLAIKYEVKFFVAHPNCQQQLTMMWYENLSGLRQQSIAVKFLAVFVSIIGLFLAIIAYWIAPCSKLGRTLRSPFMK	387
Human_TRPC1	300	LLEERNLSRLKLAIKYQKQFVVSQNCQQQLNTVWFQMSQYRRKPTCKIMTIVTVGIFWVLSLCYLIAPKSPFGRIIHTPFMK	386
Human_TRPC4	279	EEQSGNDLARKLAKIAKYRQKFEVFAQPNCCQLLASRWYDEFGWRRRHVAVKMTVCFIIGLFFPVFVSCYLIAPKSPGLGFIKPFK	365
Human_TRPC5	280	DPQKYHDLAKLAKVAIKYHQKFEVFAQPNCCQLLATLWYDGFPGWRRKHVVKLLTMTIGFLFPLMSIAYLISPRSNLGLFIKPFK	366
Mouse_TRPC2	578	FEEGIPNLRRLAVNYNQKQFVAHPICQQVLSIWCNGLAGWRGSTTIWKLFAFLIFTMPLFCIGYWLAPKSQLGRLLKIPVLK	664
Human_TRPC3	374	FVAHAASFTIFLGLLVFNASDRFEGITLTPNITVTDYPKQIFRVKTTQFTWTEMLIMVWV LGMWSECKELWLEGPREYILQLWNLV	460
Human_TRPC6	443	FVAHAASFTIFLGLLVFNASDRFEGITLTPNETSTDNAKLFRMKTSCFSWMEMLIISWVIGMIWAECKE IWTGPKREYLFELWNLV	529
Human_TRPC7	388	FVAHAYSFTIFLGLLVFNASDRFEGVKTLPNETFTDYPKQIFRVKTTQFSWTEMLIMKVV LGMWSECKE IWEQPREYLVLRNLV	474
Human_TRPC1	387	FIIHGASVFTFLLLNLVSLVYNEDKKN-----TMGPALEIDYLLLWIIGMIWSDIKRLVYEGLEDLEESRNLQ	458
Human_TRPC4	366	FICHTASYLTFLLMLLSAQHIDRSDLN-----RQGPPTIVVEWMLPWWLGFIVGEIKQMWDGGLQDYIHDWVNL	437
Human_TRPC5	367	FICHTASYLTFLLMLLSAQHIVRTDLH-----VQGPPTIVVEWMLPWWLGFIVGEIKEMWDGGLQDYIHDWVNL	438
Mouse_TRPC2	665	FLLSHASYLWFLFILLGESLVM-----E-----TQLSTF-KGRSLSVWETS LHMVWTFGLWFECKEWTIEGLRSYLLDWWNFI	737
Human_TRPC3	461	DFGMLSIFIAAFTARFLAFLQATKAQYVDSVYQESDLSVTLPEEIQYF-TYARDKWLPSDPQISEGLYAI AVVLSFSRIAYIILP	546
Human_TRPC6	530	DFGMLAIFAASFTIARFMAFWHASKAQSIIIDANDTKDLTKVTLGDNVVKY-NLARIKWDPSDPQISEGLYAI AVVLSFSRIAYIILP	615
Human_TRPC7	475	DFGMLSIFVASFTARFMAFLKATEAQLYVDQHVQDDTLHNVS LPPVAVYF-TYARDKWLPSDPQISEGLYAI AVVLSFSRIAYIILP	560
Human_TRPC1	459	SFVMNSLYLATFALKVVAHNK-----PHDFADRKWDVAFHPTLVAEGLFAFANVLSYLRIFMFT	518
Human_TRPC4	438	DFVMNSLYLATISLKIIVAVK-----YSAALNPRESWDMWHTLVAEALFAIANIFSLRILISLFT	497
Human_TRPC5	439	FAMNSLYLATISLKIIVAVK-----YNGSRPREWEMWHTLVAEALFAIANIFSLRILISLFT	498
Mouse_TRPC2	738	DVVISLVSALFALRLLLAGLA-----YMHCRD-----ASDSTTCRYFTTAERSEWRTEDPQLAEVLFVAVTSMLSFTRLAYIILP	812
Human_TRPC3	547	ANESFGPLQISLGRVTKDIFKFMVLFIMVFFAFMIGMFI LYSYLLGA-----KVNAAFTTVEESFKTLFWSIFGLSE	618
Human_TRPC6	516	ANESFGPLQISLGRVTKDIFKFMVLFIMVFFAFMIGMFI LYSYLLGA-----KQNEAFTTVEESFKTLFWSIFGLSE	687
Human_TRPC7	661	ANESFGPLQISLGRVTKDIFKFMVLFIMVFFAFMIGMFI LYSYLLGA-----KYNPAFTTVEESFKTLFWSIFGLSE	632
Human_TRPC1	519	NSHILGLPLQISMGQMLDQFGKFLGMLVLFSTFTIGTLQYDK--GYTSKEQKDCVGI FCEQSNDFHSFIGTCFALFWYI PSLAH	603
Human_TRPC4	498	ANSHLGLPLQISLGRMLLDILKFLFIYCLVLLAFANGLNQLYFYYEET--KGLTCKGIRCEKQNN-AFSTLFTLQSLFWSIFGLI-	579
Human_TRPC5	499	ANSHLGLPLQISLGRMLLDILKFLFIYCLVLLAFANGLNQLYFYYEETRAIDEPNNCKGIRCEKQNN-AFSTLFTLQSLFWSIFGLL-	583
Mouse_TRPC2	813	AHESLGLTQISIGKIMDDMIRFMFILMILTLAFCLGLNNIYVPYQES-----E---KLGNFNETFQFLFWTFMGME	881
Human_TRPC3	619	--VTSVVLKYDHKFIENIYGVLYGIVNVTMVVLLNMLIAMINSSYQEI EDDSDVEWKFARSKLWLSYFDDGKTLPPFPNLPVSPKS	703
Human_TRPC6	688	--VKSVYINYNHKFIENIYGVLYGIVNVTMVI LNLMLIAMINSSYQEI EDDADVEWKFARAKLWLSYFEEGRTPVFPNLPVSPKS	772
Human_TRPC7	633	--VISVVLKYDHKFIENIYGVLYGIVNVTMVVLLNMLIAMINSSYQEI EEDADVEWKFARAKLWLSYFEEGRTPVFPNLPVSPKS	717
Human_TRPC1	604	VAIFVTRFSYGEELQSFGAVIVGTYNVVVVVILTKLLVAMLHKSQLIANHEDEKWKFAKRLWLSYFDDGKTLPPFPNIIIPSPKT	690
Human_TRPC4	580	NLYVTNVKARHEFTEFVGTATMFTYNNVLSLVLLNMLIAMMNSYQLIADHADIEWKFAKRLWLSYFEEGGTLPTFVNIIPSPKS	665
Human_TRPC5	584	NLYVTNVKARHEFTEFVGTATMFTYNNVLSLVLLNMLIAMMNSYQLIADHADIEWKFAKRLWLSYFEEGGTLPTFVNIIPSPKS	669
Mouse_TRPC2	882	--HTVVDM-PQFLVPEFVGRAMYIFETIVMVI LNLMLIAMNITNSFQKIEDDADVEWKFARSKLWLSYFREGKTLPPFPNIIIPSPKA	965
Human_TRPC3	704	FVYFIMRIVN---FPKCRRRRLQKDIEMGMGNSKSRNLN-----LFTQNSRVFESHFNLSILNQPTRYQQIM	767
Human_TRPC6	773	LFYLLKLLKWKWSELFCQHKGFQEDAEMNKINEEKLGLIGSHEDLSKLSLDKQVGHNKQPSIRSSDFHLSNFKPTRYQKIM	859
Human_TRPC7	718	FYYLIMRINKMLIKLCKSKAKSCENDLEMGLNSKFKKT-----RYQ-AGMRNSENLTANNTSNKPTRYQKIM	784
Human_TRPC1	691	ICYMISLSLKWICSHTSKGVKQRQNSLKE-----WRNLKQKRDENYQKVM	735
Human_TRPC4	666	LWYLIKRWIWLHCKKMK-----RRKPEFSGT-----IGR-----RAADNLRHHQYQEVQM	710
Human_TRPC5	670	FLYLGWNFNTFCPKRDPDGRRRRNLRS-----FTE-----RNADSLIQNHQYQEV	717
Mouse_TRPC2	966	AFYLVRRIFRFLCCGSCKCAKKSDDYPII-----GFTTNP GARAGSAGEG-----RVSYRLRVI	1020
Human_TRPC3	768	KRLIKRYVVLKQVQDKENDEV--NEGELKEIKQDISSLRYLELLE-----DKSQATEELA-----LIHKLSE--K	827
Human_TRPC6	860	KRLIKRYVVLKQVQDKESDEV--NEGELKEIKQDISSLRYLELLE-----EKSQNTEDA-----ELIRELGE--K	919
Human_TRPC7	785	KRLIKRYVVLKQVQDREDEV--NEGELKEIKQDISSLRYLELLE-----EKSQATGEA-----DLIQLSE--K	844
Human_TRPC1	736	CVLHRYLVTSMRQKMQSTDQ-ATVENLNLQRDLSKFRNEIRDLLGPRGTSKYAMFYPRN-----	793
Human_TRPC4	711	RNLVKRYVAAMIRDAKTEEG-LTEENFKEIKQDISSFRFEVGLLRLGSKLSTIQSANASKSSNSADSDSEKSDSEKSKDKKKNFSL	796
Human_TRPC5	718	RNLVKRYVAAMIRNSKTHEG-LTEENFKEIKQDISSFRFEVLDLLGNRKHPRSFSTSSTEL---SQRDDNDGSGGARAKSKSVS-	798
Mouse_TRPC2	1021	KALVQRVYIETARREFEETRRKDLGNRLTELTKTYSRLQSEVAVSQVKNLAAGGAPRPDASIL--S-----RYITVRNSFQN	1096
Human_TRPC3	828	LNP SML-----RCE-----	836
Human_TRPC6	920	LSMEPN-----QEETNR-----	931
Human_TRPC7	845	FGKNLN-----KDLRVNKGKDI-----	862
Human_TRPC1	797	FDLTTLIHPRSAAIA-SERHNISNGSALVVQE---PP-----REKQ	833
Human_TRPC4	799	FNLGCK-----KKTCHGAPLIRTM---PRSSGAQGSKAESS	833
Human_TRPC5	799	FNLGCK-----KKTCHGAPLIRTM---PRSSGAQGSKAESS	833
Mouse_TRPC2	1097	LGPPTSDTPAELTMPGIVETEVSLGDDLGTGEAGAPPEGSSSS-----	1143

Figure 3 – figure supplement 5

